GRK2 regulates mitochondrial bioenergetics and impairs myostatin-mediated autophagy in muscle cells

Leandro Henrique Manfredi[1,2,3], Joshur Ang[3], Nesibe Peker[4], Ruben K. Dagda[5], and Craig McFarlane[3,6]

[1]Department of Physiology, Medical School of Ribeirão Preto, University of São Paulo, Ribeirão Preto, Brazil.

[2]Federal University of Fronteira Sul, Medical School, Chapecó, Santa Catarina, Brazil.

[3]Singapore Institute for Clinical Sciences (A*STAR), Brenner Centre for Molecular Medicine, 30 Medical Drive, Singapore 117609.

[4]School of Biological Sciences, 60 Nanyang Drive, Nanyang Technological University, Singapore 637551.

[5]University of Nevada, Reno School of Medicine, Department of Pharmacology, Howard Medical Sciences 148, Reno, NV, 89557.

[6]Department of Molecular & Cell Biology, College of Public Health, Medical and Veterinary Sciences, James Cook University, Townsville, QLD, Australia.

Leandro Henrique Manfredi: leandrohm@gmail.com

Joshur Ang Yew Loong: joshur_ang@bti.a-star.edu.sg

Nesibe Peker: NESIBE001@e.ntu.edu.sg

Ruben K. Dagda: rdagda@med.unr.edu

Craig McFarlane: craig.mcfarlane@jcu.edu.au

Running Title: Myostatin regulation of GRK2

Address correspondence to:

Dr Craig McFarlane
Department of Molecular & Cell Biology
College of Public Health, Medical and Veterinary Sciences
1 James Cook Drive
Townsville, QLD 4811
Australia
Phone: +61 7 4781 5657
Email: craig.mcfarlane@jcu.edu.au

Abstract

GRK2 is an important protein involved in β-adrenergic receptor desensitization. In addition, studies have shown GRK2 can modulate different metabolic processes in the cell. For instance, GRK2 has been recently shown to promote mitochondrial biogenesis and increase ATP production. However, the role of GRK2 in skeletal muscle and the signaling mechanisms that regulate GRK2 remain poorly understood. Myostatin is a well-known myokine that has been shown to impair mitochondria function. Here, we have assessed the role of Myostatin in regulating GRK2 and the subsequent downstream effect of Myostatin regulation of GRK2 on mitochondrial respiration in skeletal muscle. Myostatin treatment promoted the loss of GRK2 protein in myoblasts and myotubes in a time- and dose-dependent manner, which we suggest was through enhanced ubiquitin-mediated protein loss, as treatment with proteasome inhibitors partially rescued Myostatin-mediated loss of GRK2 protein. To evaluate the effects of GRK2 on mitochondrial respiration, we generated stable cell myoblasts lines that overexpress GRK2. Stable overexpression of GRK2 resulted in increased mitochondrial content and enhanced mitochondrial/oxidative respiration. Interestingly, although overexpression of GRK2 was unable to prevent Myostatin-mediated impairment of mitochondrial respiratory function, elevated levels of GRK2 blocked the increased autophagic flux observed following treatment with Myostatin. Overall, our data suggest a novel role for GRK2 in regulating mitochondria mass and mitochondrial respiration in skeletal muscle.

Keywords: Myostatin, myoblast, GRK2, Mitochondria, autophagy

Background

G protein-coupled receptor kinases (GRKs) are serine/threonine kinases initially identified to participate in the process of G protein-coupled receptor desensitization (53). GRKs comprise a family that can be partitioned into three groups through sequence homology: GRK1/7; GRK2/3 and GRK4/5/6 (54). GRK1 and 7 are found in retinal rods and cones, respectively, and GRK4 is expressed in testis, cerebellum and kidney (38, 53-55). However, ubiquitous expression of GRK2, 3, 5 and 6 is observed in mammalian tissues (53-55). These kinases can phosphorylate specific amino acid residues in the intracellular domain of activated receptors and lead to recruitment of adaptor proteins (e.g. β-arrestins) in order to attenuate intracellular G protein signaling (54, 63).

Recent studies have identified GRK2 as an emerging kinase involved in regulating different cellular process through phosphorylation and/or association with other proteins (13, 23, 26, 72). Moreover, GRK2 expression and activity is tightly regulated and is altered during several pathological conditions, for example hypertension, heart failure and inflammation (41, 49, 75). GRK2 has recently been linked to mitochondrial function and biogenesis (18). Overexpression of GRK2 has been shown to promote increased mitochondrial mass and further enhance ATP production due to the ability of GRK2 to target and phosphorylate mitochondrial proteins in HEK293 cells; whereas knockdown of GRK2 led to reduced ATP production in skeletal muscle (18). Moreover, macrophages treated with LPS exhibited enhanced GRK2 accumulation in mitochondria, which was associated with increased mtDNA copy and reduced ROS production (65). Although several studies have helped to delineate GRK2 function using different model systems, the function of GRK2 in skeletal muscle metabolism remains to be fully elucidated.

Members of the TGF-β superfamily of secreted growth factors, including GDF11 and Myostatin, have negative impact on skeletal muscle growth and maintenance (11, 45). More specifically, Myostatin has been previously shown to inhibit myoblast proliferation (58, 69), myogenic differentiation (27, 33), block protein synthesis signaling and promote a reduction in myotube size (70). Moreover, elevated levels Myostatin has been shown to promote loss of mitochondrial membrane potential and impair mitochondrial function in cancer cells (39). Importantly, Myostatin is a

potent inducer of skeletal muscle wasting and increased Myostatin activity has been observed in different atrophic conditions (1, 42, 56).

Over the past 10 years, many studies have revealed the pathological mechanisms involved in Myostatin-mediated atrophy in skeletal muscle. Specifically, McFarlane *et al*. (2006) reported that Myostatin was able to block IGF1/PI3K/Akt signaling and activate the transcription factor FoxO1, which increases the expression of MAFbx/Atrogin-1 and MuRF1/Trim63 (44), two well-known muscle-specific E3 ligases that are associated with muscle atrophy (2, 12). Myotubular atrophy has also been noted in human myotubes upon treatment with excess Myostatin (32, 40), which was associated with increased levels of Atrogin-1 and MuRF1 (40). Additional work has revealed that Myostatin signals through Smad3 to increase FoxO1 and Atrogin-1 to promote the ubiquitination and subsequent loss of critical sarcomeric proteins, such as myosin heavy chain (MyHC), during muscle wasting (40).

As GRK2 and Myostatin have been shown to regulate mitochondrial function we sought to determine a potential role for Myostatin in regulating GRK2 and subsequent mitochondrial respiration in skeletal muscle. In this report, we show that Myostatin targets and suppresses GRK2 protein levels in muscle cells, through a mechanism involving the ubiquitin-proteasome pathway. In the present study, we find that Myostatin treatment leads to impaired mitochondrial respiration, which was associated with mitochondrial fragmentation, enhanced autophagic flux and reduced mitochondrial content in muscle cells. We have further unraveled a novel role for GRK2 in regulating mitochondrial respiration in muscle cells. Overexpression of GRK2 in myoblasts also led to increased mitochondrial fragmentation; however, unlike Myostatin, GRK2 overexpression was associated with enhanced mitochondrial respiration and increased mitochondrial mass. Surprisingly, while overexpression of GRK2 was not able to overcome the negative effect of excess Myostatin on mitochondria respiration; elevated GRK2 levels resulted in increased mitochondria content and a reduction in the overt-autophagic flux noted in the presence of excess Myostatin. Overall, these data reveal a novel role for GRK2 in regulating mitochondrial respiration and mass in muscle cells and reveal that increased expression of GRK2 may act to compensate, at least in part, for the loss of mitochondria noted upon Myostatin treatment.

Materials and Methods

Cell culture and treatments

Mouse C2C12 myoblasts were obtained from American Type Culture Collection and their maintenance has been previously described (43). C2C12 myoblasts were expanded in myoblast proliferation medium (10% FBS, 1% P/S, and DMEM; Invitrogen) and differentiated into myotubes through serum withdrawal in differentiation medium (DMEM, 2% HS, and 1% P/S; Invitrogen) for 96h, to ensure complete differentiation of cultures. Doxycycline (2μg/ml) was added together with differentiation medium in order to induce the stable overexpression of GRK2. Recombinant Myostatin protein (Mstn) was purified from *E. coli* (62) and was used at a concentration of 3μg/ml for cell treatments, unless otherwise stated. For proteasome inhibitor studies C2C12 myotubes were treated with 3μg/ml recombinant Mstn for a total period of 24h. To block the activity of the proteasome MG132 (Sigma, St. Louis, MO) and Epoxomicin (Epox; Sigma) chemicals were added to C2C12 myotubes at 10μm and 100nM final concentrations, respectively, 10h prior to harvesting the cells. The difference in total GRK2 seen in the absence of presence of the proteasome inhibitors represents the content of GRK2 that is being degraded through the ubiquitin-proteasome system (29, 34). One independent experiment was performed with MG132 with 3 biological replicates and one confirmatory experiment was performed with Epox.

To block the lysosomal pathway, 100μM of chloroquine (Sigma) was added to myotubes in the presence or absence of Mstn (3μg/ml) for 12h. The difference in the protein levels of LC3-II between samples treated with and without chloroquine represents the level of autophagic flux in the cells (30, 77). Two different experiments were performed, each with one biological replicate.

Generation of GRK2 stable cell lines

Full length murine *Grk2* cDNA (NM_130863.2) was PCR-amplified using the following primers: 5' - CC ACC GGT ATG CAG AAG TAT CTG GAG GAC CGA - 3' and 5' - ACC TGT ACA TCA GAG GCC GTT GGC ACT GCC ACG - 3' and cloned into the pGEM-T easy cloning vector (Promega). After sequence verification, *Grk2* was subcloned into the doxycycline-inducible PEM777 expression vector (28). *Grk2*-PEM777 or empty-PEM777 (Control) were transfected into C2C12 myoblasts and cells using Lipofectamine 2000 (Invitrogen), as previously described (28). Following 3 days

of selection with puromycin (1μg/ml), stably transfected cells were harvested and expanded for further experimental procedures in the presence of 2μg/ml doxycycline.

Assessment of mitochondrial respiration

Mitochondrial respiration was assessed *in vitro* using the XF^{e}24 extracellular flux analyser, and the XF Cell Mito Stress and Glycolysis Stress Test Kits, as per the manufacturer's protocol (Agilent Technologies, Santa Clara, CA, USA), and as described previously (20, 52). For assessment of real-time mitochondrial respiration of myotubes, myoblasts were seeded (10,000 cells/well) onto XF^{e}24 cell culture microplates and differentiated to form myotubes, as outlined above, in the presence of 100ng/ml doxycycline for 48h. Cells were then treated with either 2μg/ml recombinant Mstn protein or an equal volume of dialysis buffer (Control) for a further 24h. The XF^{e}24 sensor cartridge was hydrated overnight at 37˚C in a non-CO_2 incubator. 30 minutes prior to assay run, differentiation medium was replaced with Assay Medium (Agilent Technologies, Santa Clara, CA, USA) and cells were incubated at 37˚C in non-CO_2 incubator. Three measurements of oxygen consumption rate (OCR) and extracellular acidification rate (ECAR) were recorded pre- and post-injection of 1 μM Oligomycin (Oligo), 0.5μM FCCP and 0.5μM Antimycin/Rotenone (Ant/Rot) (Agilent Technologies, Santa Clara, CA, USA) (14).

Using the Wave Desktop 2.3 software, seven parameters of mitochondrial respiration, basal OCR, ATP-linked OCR, OCR due to proton leak, maximal OCR, spare respiratory capacity, non-mitochondrial OCR and ECAR, were calculated from the bioenergetic profiles obtained from the XF^{e}24 extracellular flux analyzer, which has been outlined in detail previously (22). Briefly, basal OCR refers to the total baseline cellular respiration rate and includes respiration due to ATP production, proton leak (leak of protons across the inner mitochondrial membrane) and oxygen consumption due to non-mitochondrial processes (22). ATP-linked oxygen consumption is determined through the addition of the ATP synthase inhibitor oligomycin, which effectively shuts down ATP production due to oxidative phosphorylation. Any residual mitochondrial respiration/oxygen consumption noted at this point can then be attributed to proton leak (22). Maximal OCR is determined through the addition of the proton ionophore (uncoupler) FCCP, which increases inner mitochondrial membrane permeability to protons, increasing oxygen consumption and allowing for the assessment of the maximal oxygen consumption/respiration possible in the cells (22).

196 Spare respiratory capacity is calculated through determining the difference between
197 basal OCR and maximal OCR in the cells and this reflects the amount of extra oxygen
198 consumption/ATP-production that can be achieved by the cells in response to increased
199 energy demand (7). Non-mitochondrial respiration is the oxygen consumption due to
200 non-mitochondrial processes. Although not well defined, this has been attributed to
201 such processes as hydrogen peroxide production (3) and the enzymatic activity of
202 oxygenases (4). Assessment of extracellular acidification rate (ECAR) is primarily a
203 measure of acid release and is related to lactic acid formation during glycolysis (15).
204 Basal respiratory capacity was recorded at the third readout of OCR just prior to
205 oligomycin injection, whereas mitochondrial respiration due to proton leak was
206 recorded at 6^{th} OCR readout, which is just prior to FCCP injection. Maximal respiration
207 was recorded as the highest OCR measurement following FCCP injection. ATP-linked
208 respiration and spare respiratory capacity were calculated by subtracting OCR due to
209 treatment with oligomycin from basal respiration and basal respiration from maximal
210 respiratory capacity, respectively. Non-mitochondrial respiration was taken as the
211 minimum OCR measurement after injection of Ant/Rot and was subtracted from all
212 respiratory calculations. Values were normalized to total protein content. Two
213 independent experiments were performed to assess mitochondrial respiration, each
214 containing 5 biological replicates. Three measurements per timepoint were assessed.
215
216 *RNA extraction and quantitative real time PCR (qPCR)*
217 Isolation of total RNA from C2C12 myotubes was performed using TRIZOL
218 reagent, as per the manufacturer's instructions (Invitrogen, Carlsbad, CA). Synthesis of
219 cDNA was achieved using the iScript system (Bio-Rad Laboratories, Inc., Hercules,
220 CA), according to the manufacturer's protocol. Quantitative real-time PCR (qPCR) was
221 undertaken using the SsoFast EvaGreen Supermix (Bio-Rad) and the CFX96 Real-Time
222 PCR system (Bio-Rad). Transcript levels of target genes were normalized against the
223 expression of the housekeeping gene *Gapdh*. Relative fold change in expression was
224 calculated using the ΔΔcycle threshold (ΔΔCT) method. The sequences of the primers
225 used in this manuscript are given in Table 1. All oligos pertaining to this study were
226 purchased from Sigma Aldrich (Singapore). All qPCR in this study was performed once
227 with 3 biological replicates and two technical replicates per sample/treatment.
228
229 *Immunoblotting (IB)*

Proteins were isolated from myoblasts and myotubes using protein lysis buffer [50mM Tris, (pH 7.5), 250mM NaCl, 5mM EDTA, 0.1% NP-40, Complete protease inhibitor cocktail (Roche, Indianapolis, MN), 2mM NaF, 1mM Na_3VO_4, and 1mM phenylmethylsulfoxide (PMSF)]. Proteins were quantified using Bradford reagent (Bio-Rad). A total of 25 µg of each protein lysate was resolved on 4-12% BIS-TRIS precast gels (Invitrogen). Proteins were then transferred onto nitrocellulose membrane using either the Invitrogen iBlot® 2 dry transfer system or the XCell II SureLock™ wet transfer system (Invitrogen, Carlsbad, CA, USA). Membranes were then blocked overnight at 4°C in 5% milk in 1× Tris-buffered saline-Tween 20 (TBST) and proteins were hybridized with specific primary antibodies for 3h in 5% milk/1× TBST. Membranes were then washed in 1× TBST, 5 times for 5 min each, before and after 1h incubation with a 1:5,000 dilution of respective secondary antibodies, either goat anti-rabbit horse radish peroxidase (HRP) (Catalogue No:1706515; Bio-Rad, Hercules, CA, USA) or goat anti-mouse HRP (Catalogue No:1706516; Bio-Rad, Hercules, CA, USA) antibodies. Antibody-bound proteins were detected using Western Lightning Chemiluminescence Reagent Plus (PerkinElmer, Boston, MA) and autoradiography films (Kodak). Protein levels were quantified and analyzed using the GS-800 calibrated densitometer (Bio-Rad) and analyzed using Quantity One imaging software (Bio-Rad). Details of the primary and secondary antibodies used in this study are provided in Table 2. The specificity of the anti-LC3B antibody has previously been demonstrated using a commercially available recombinant protein by Koukourakis *et al*., (2015) (31). The anti-MFN1 antibody has been previously used to demonstrate increased levels of Mfn1 protein in liver tissue of high fat diet fed mice and in hepatocytes that display a swollen mitochondrial morphology (25). Previous target-specific siRNA knockdown studies have confirmed the specificity of the anti-P62 (76), anti-GRK2 (61), anti-PARKIN (36, 67), anti-MFN2 (79), anti-DRP1 (37) and anti-FIS1 (46) antibodies used in the current study. The number of experimental and biological replicates for IB analysis are detailed in relevant figure legends.

Mitotracker Red staining and assessment of mitochondria morphology using confocal microscopy

Following 72h doxycycline (2µg/mL) induction C2C12 myoblasts were seeded onto 8-well Permanox chambered slides, at a density of 5,000 cells per well. After overnight attachment, myoblasts were treated with recombinant Mstn protein (3µg/ml)

for 24h. To identify mitochondria, myoblasts were incubated for 30 min with 200 nM Mitotracker Red (CMX red Rosamine-based Mitotracker dye, Invitrogen). Cells were washed 3 times with PBS and subsequently fixed with paraformaldehyde (4%) in DMEM for 15 minutes. After fixation, cells were washed 3 times and were then mounted using SlowFade antifade reagent containing DAPI and analyzed using confocal microscopy (Nikon, 60X).

To analyze mitochondrial morphology in control and GRK2 overexpressing C2C12 cells in the presence or absence of Mstn protein, the indices of mitochondrial interconnectivity (area/ perimeter ratio per mitochondrion), which is a measure of mitochondrial elongation, were quantified for each mitochondrion using the well-validated NIH Image J macros (Mitochondrial and Mitophagy Morphology macros (available at http://imagejdocu.tudor.lu/), as previously described (59), with minor modifications. The particular Image J macro was originally described by Dagda *et al*., 2009 (6) and importantly, has been used by several investigators since that time (5, 19, 66). Moreover, one recent study by Wiemerslage and Daewoo, (2016), further validated the Mitochondrial Morphology macro in dopamine neurons and analyzed the relationship and interdependency of individual parameters quantified by the macro (number of mitochondria, area, elongation, interconnectivity) under various conditions using principle component analysis (74). To quantify mitochondrial interconnectivity in C2C12 cell, between 10-15 high resolution RGB images (TIFF, 1020 x 1020 pixels) were captured for each condition using confocal microscopy and were analyzed for mitochondrial morphology. In order to account for possible swelling of mitochondria, the area/perimeter were normalized for the minor axis of an ellipse that was "fitted" onto each mitochondrion analyzed by the macro. The interconnectivity ratio [(area/perimeter ratio)/minor axis] per cell were averaged for 50-100 mitochondria per cell, and subsequently averaged for the entire population size for each experimental condition (25-30 cells). A low average interconnectivity ratio for a specific experimental condition (e.g. Mstn treated cells relative to control untreated cells) is indicative of mitochondrial fragmentation (fission).

Mitotracker Green Staining

Following 72h doxycycline induction C2C12 myoblasts were seeded onto 6-well plates, at the density of 15,000 cells/cm^2. The next day, cells were treated with 2μg/ml recombinant Mstn protein or an equal volume of dialysis buffer (Control) and incubated

298 at 37˚C, 5% CO_2. After 24h, myoblasts were stained with 150nM MitoTracker® Green
299 FM (Thermo Fisher Scientific, Waltham, MA, USA) for 20 minutes at 37˚C. Cells were
300 washed twice with PBS and harvested in conical tubes by centrifuging at 300xg for 1
301 minute. Cell pellets were resuspended in PBS and FACS analysis was performed to
302 detect MitoTracker® Green FM fluorescence intensity using the FACSCanto™ II flow
303 cytometry system (BD Biosciences, Franklin Lakes, NJ, USA). Fluorescent intensity of
304 10,000 events from 3 replicate wells per experimental group were detected using the
305 FITC channel and represented as mean fluorescent intensity (MFI). Two technical
306 replicates were performed.
307
308 *Statistical Analysis*
309 Statistical analysis was performed using two-tail Student's-t-test and ANOVA,
310 using the Bonferroni post-hoc test. Data are expressed as mean ±SEM and results were
311 considered significant at $p<0.05$. A description of experiment replicates is provided in
312 relevant figure legends.

Results

Mstn promotes the loss of GRK2 protein via the Ubiquitin Proteasome Pathway (UPP)

Initially we investigated whether or not Myostatin can modulate GRK2 expression. Immunoblot (IB) analysis revealed that treatment of C2C12 myotubes with recombinant Myostatin protein (Mstn) resulted in a ~70% decrease in GRK2 protein content after 24h treatment (Fig. 1A). We further noted both a time- and dose-dependent decrease in GRK2 protein levels in both C2C12 myoblasts and myotubes following treatment with Mstn (Fig. 1B and 1C). However, Mstn-induced loss of GRK2 protein was more pronounced in C2C12 myotubes compared to Mstn-treated C2C12 myoblasts (Fig. 1B & 1C).

Since Mstn has been shown to increase the activity of the UPP to promote loss of skeletal muscle proteins (44), we next evaluated whether or not Mstn promotes the loss of GRK2 protein through the UPP. As shown in Fig. 1D and 1E, treatment of C2C12 myotubes with Mstn resulted in reduced protein levels of GRK2. However, treatment of C2C12 cells with two different specific proteasome inhibitors (MG132 and Epoxomicin) was able to partially rescue the loss of GRK2 protein observed following Mstn treatment. (Fig. 1D & 1E).

Taken together, these data suggest that Mstn is able to promote loss of GRK2 protein, through activation of the Ubiquitin Proteasome Pathway (see summary; Fig. 4).

GRK2 and Mstn have differential effects on mitochondrial mass and OXPHOS gene expression in myotube cultures

It has been previously reported that GRK2 can target mitochondria in HEK293 cells to increase mitochondrial function and enhance ATP generation (18). On the other hand, Myostatin is a myokine that promotes mitochondrial dysfunction and loss (39). Thus, we next sought to determine: 1) the effect of GRK2 on mitochondrial mass and respiration in muscle cells, and 2) whether or not GRK2 may play a role in Mstn regulation of mitochondria. To facilitate this, we generated doxycycline-inducible GRK2 overexpressing C2C12 cells, with GRK2 overexpression in myotubes subsequently confirmed through both qPCR (Fig. 2A) and immunoblot analysis (Fig. 2B). It is worth noting that despite significant over expression of GRK2, Mstn treatment was still able to reduce GRK2 protein levels, but not *Grk2* mRNA expression, in GRK2-overexpressing C2C12 myotubes (Fig. 2A & 2B). However, the levels of GRK2

protein remained elevated above endogenous levels compared to the control cell line, despite excess Mstn treatment (Fig. 2B).

Initially we assessed mitochondrial mass through MitoTracker Green FM staining and subsequent FACS analysis. Results revealed a reduction in mitochondrial mass in response to Mstn treatment and an increase in mitochondrial mass upon overexpression of GRK2. (Fig. 2C). Conversely, a significant increase in mitochondrial mass was observed in GRK2-overexpressing myoblast cultures upon treatment with exogenous Mstn (Fig. 2C). Despite the increase in mitochondrial mass noted in control GRK2 overexpressing cells, the expression of critical OXPHOS genes (which encode for subunits of Complex I and Complex IV) was unaltered between untreated control and GRK2 overexpressing myotube cultures (Fig. 2D). Unexpectedly, the expression of the OXPHOS genes tended to increase in response to Mstn treatment (Fig. 2D), with the greatest increase in OXPHOS gene expression noted in Mstn treated GRK2 overexpressing cells, when compared to Mstn treated control cells (Fig. 2D).

GRK2 and Mstn influence mitochondrial fission and fusion in myotube cultures

Next, we investigated the role of GRK2 and Mstn in mitochondrial structure/dynamics through analysis of mitochondrial fission and fusion markers. Western blot analysis revealed a significant reduction in the protein levels of mitochondrial fusion markers, MFN1 and MFN2, upon Mstn treatment, in both control and GRK2-overexpressing C2C12 myotubes (Fig. 3A & 3B). Furthermore, a significant increase in the levels of the mitochondrial fission marker proteins Drp1 and Fis1, and the mitochondrial E3 ligase PARKIN were observed upon Mstn treatment of control cells, with significantly increased levels of both Fis1 and PARKIN also noted in Mstn treated GRK2-overexpressing C2C12 myotubes (Fig. 3A & 3B). These data suggest that Mstn treatment is associated with reduced mitochondrial fusion and increased mitochondrial fission in C2C12 myotube cultures. A significant increase in the levels of Fis1was also noted in untreated GRK2-overexpressing C2C12 myotubes, when compared to untreated control cells; however, in contrast to what was observed following Mstn treatment, the levels of Drp1 and Parkin remained low and were in fact slightly reduced in untreated GRK2-overexpressing C2C12 myotubes, when compared to untreated controls (Fig. 3A & 3B). Interestingly, significantly increased levels of both MFN1 and MFN2 were observed in untreated GRK2-overexpressing C2C12 myotubes, when compared to controls (Fig. 3A & 3B).

We next stained control and GRK2-overexpressing myoblasts, treated with or without Mstn protein, with Mitotracker Red to visualize mitochondria and to assess for qualitative changes in mitochondria morphology (Fig. 3C). Through using semi-automated macros that determine the mitochondrial interconnectivity ratio (area/perimeter normalized to the minor axis of an ellipse) (59), we observed that untreated cells contained interconnected mitochondria, as evident by long tubular mitochondrial networks (Fig. 3C & 3D). However, Mstn treatment of cells led to a robust fragmentation of mitochondrial networks and a decreased mitochondrial interconnectivity ratio (Fig. 3D). Paradoxically, inducible expression of GRK2 also resulted in a decreased mitochondrial interconnectivity ratio per cell (Fig. 3D). The combination of GRK2 overexpression and Mstn treatment resulted in a partial reversal of mitochondrial fragmentation induced by GRK2 alone, back to levels similar to cells treated with Mstn alone. However, the overall levels of fragmentation were still significantly lower when compared to untreated control cells (Fig. 3D). Based on the image analysis, our data shows that both GRK2 and Mstn treatment induce mitochondrial fragmentation/fission; although the molecular mechanism through which both proteins promote reduced mitochondrial interconnectivity is distinct, as per our Western blot data (altered MFN1/2 levels and increased Drp1 vs. Fis 1 levels; Fig. 3B).

GRK2 overexpression prevents the increased autophagic flux observed in response to Mstn treatment

It is well established that excess Myostatin leads to increased autophagy (35, 73). Mitophagy is the selective process by which damaged/defective mitochondria are targeted for lysosomal-mediated degradation (30). Once different outer mitochondrial membrane-localized proteins are ubiquitinated, by E3 ligases including Parkin, mitochondria are “flagged” and targeted for degradation by the ubiquitin-binding adaptor protein P62/SQSTM1, which in turn associates with LC3 in the autophagosome, leading to the engulfment and degradation of mitochondria (51). During this process, the LC3 isoform I is conjugated to phosphatidylethanolamine to form a membrane-bound form of LC3, termed LC3-II, which remains bound to autophagosome until it is targeted for degradation by the lysosome (68). To determine whether or not GRK2 plays a role in autophagy, we next assessed autophagic flux in dialysis buffer and Mstn treated control and GRK2-overexpressing cells, in the presence or absence of chloroquine, a lysosomotropic agent that inhibits autophagy (64). As observed in Fig.

3E, chloroquine treatment resulted in the accumulation of both p62 and LC3-II in control cells and of LC3-II in GRK2-overexpressing cells, consistent with a blockade in autophagy (Fig. 3E). However, upon Mstn treatment, we observed a noticeable increase in p62 and LC3-II accumulation in chloroquine treated control cells, when compared to dialysis buffer treated controls (Fig. 3E), indicating increased autophagic flux in response to Mstn treatment. Interestingly, no difference in p62 or LC3-II accumulation was observed in Mstn treated GRK2-overexpressing cells in the presence of chloroquine, when compared to control cells treated with chloroquine. These data suggest that over expression of GRK2 prevents the overt-autophagic flux induced upon Mstn treatment in myotube cultures, which is consistent with the increased mitochondrial mass noted in Mstn treated GRK2 overexpressing myoblasts (Fig. 2C).

Mstn treatment impairs, while GRK2 overexpression increases, mitochondrial respiratory capacity in C2C12 myoblasts

We next evaluated mitochondrial respiration in control and GRK2-overexpressing myotubes by measuring OCR and ECAR by employing the XF^{e}24 Extracellular Flux Analyser (Agilent Technologies). In this system, OCR is used to measure real-time mitochondrial respiration and ECAR is used to measure glycolysis (14). Extracellular flux analysis revealed a significant reduction in overall OCR in myotubes treated with Mstn (Fig. 3F & 3G). Subsequent quantification of real-time OCR data revealed a significant reduction in basal OCR, ATP-linked OCR, which reflects ATP production through oxidative phosphorylation, maximal OCR (maximal respiration possible in the cells) and spare respiratory capacity (amount of extra ATP-production that can be achieved by the cells in response to increased energy demand) following Mstn treatment (Fig. 3G). In addition, Mstn treatment resulted in a significant reduction in the OCR due to proton-leak (leak of protons across the inner mitochondrial membrane) as well as non-mitochondrial respiration, which is OCR due to non-mitochondrial processes in the cells (Fig. 3G). Interestingly, GRK2 overexpression led to a significant increase in the OCR of C2C12 myotubes (Fig. 3F & 3G), with a significant increase in basal OCR, maximal OCR, ATP-linked OCR and spare respiratory capacity noted upon overexpression of GRK2 (Fig. 3G), suggesting that elevated GRK2 has a positive effect on cellular respiration, enhancing maximal cell respiration and the potential to produce extra ATP in times of increased energy demand (Spare respiratory capacity). Importantly, we noted a statistically significant, albeit only

449 a very modest, reversal of Mstn-mediated repression of maximal OCR and spare
450 respiratory capacity upon overexpression of GRK2 (Fig. 3G). The graph shown in Fig.
451 3H is a visual representation of the metabolic phenotype in cells and reveals that
452 untreated GRK2-overexpressing cells are more aerobic, when compared to untreated
453 control cells (Fig. 3H). In addition, analysis revealed that Mstn treatment resulted in a
454 robust increase in glycolysis and decreased aerobic respiration in myotube cultures, as
455 evident by the increase in ECAR and concomitant reduction in OCR, respectively.
456 Taken together these data suggest that while overexpression of GRK2 has a positive
457 effect on mitochondrial respiration and can block Mstn-mediated autophagy in muscle
458 cells, overexpression of GRK2 is not able to completely reverse the detrimental effect of
459 Mstn on mitochondrial respiration (see summary; Fig. 4).
460

Discussion

In this report, we have undertaken studies to explore GRK2 function in muscle cells and the role that GRK2 plays in Myostatin-mediated regulation of mitochondrial respiration. Herein, we have shown that overexpression of GRK2 in muscle cells leads to increased mitochondrial mass and respiration, as measured through oxygen consumption rate. In addition, our data suggests that GRK2 modulates mitochondrial dynamics, as inducible overexpression of GRK2 altered the levels of key regulators of mitochondrial fission and fusion and ultimately resulted in increased mitochondrial fragmentation. Excess Mstn also altered the levels of mitochondrial fusion and fission markers and further led to increased mitochondrial fragmentation; however, in contrast to what was observed in GRK2 overexpressing myoblasts, excess Mstn resulted in reduced mitochondrial mass, increased autophagic flux and impaired mitochondrial respiration in muscle cells. Importantly, although elevated GRK2 levels was able to prevent the Mstn-mediated increase in autophagic flux, overexpression of GRK2 was unable to rescue the impaired mitochondrial respiration noted upon Mstn treatment. Our findings support a beneficial role for GRK2 in increasing mitochondrial respiration and preventing overt autophagy and loss of mitochondrial mass in skeletal muscle cells.

As we have observed that Mstn represses the protein levels of GRK2 (Fig. 1 & 2), but has no significant inhibitory effect on *Grk2* mRNA expression (Fig. 2A), we propose that Mstn regulates GRK2 levels post-transcriptionally. This is quite consistent with the involvement of the ubiquitin-proteasome pathway (UPP) in Mstn-induced repression of GRK2 protein levels that we have described (Fig. 1D & 1E). Given this, we propose that GRK2 protein may be targeted for degradation through the UPP in response to Mstn treatment (Fig. 4). Myostatin has been shown to upregulate both Atrogin-1 and MuRF1 E3 ligases to promote UPP-mediated protein degradation in conditions of muscle wasting (40, 44), thus we speculate that Myostatin may signal through the E3 ligases Atrogin-1 and/or MuRF1 to target and degrade GRK2 protein. Moreover, Salcedo *et al*., 2006 have revealed that in HeLa and HEK-293 cells GRK2 is targeted by the E3-ubiquitin ligase Mdm2 for degradation through the UPP upon β_2-AR stimulation (60). Given that Mdm2 is expressed in muscle cells (17) it is quite possible that Myostatin may signal through Mdm2 to regulate GRK2. However, future studies will need to be performed to further clarify the specific molecular mechanism(s) through which Myostatin targets and represses GRK2 protein levels in muscle cells.

It is important highlight that we noted a more pronounced repression of GRK2 protein levels in Mstn treated myotube cultures, when compared to myoblast cultures (Fig. 1B & 1C). Although the exact reason for this phenomenon remains to be defined, it is noteworthy to mention that the levels of the canonical Myostatin signaling target Smad3 (24) are increased during myogenic differentiation (9, 78). Thus, we speculate that the greater inhibitory effect of Myostatin on GRK2 may be due to increased availability of Smad3 and subsequent downstream signaling in myotube cultures. However, future studies will need to be undertaken to confirm this.

Fusco *et al.* (2012), have recently shown that GRK2 overexpression in HEK-293 cells led to increased ATP production and mitochondrial biogenesis and that loss of GRK2 from skeletal muscle *in vivo* reduces ATP production (18). In agreement with this, we find increased mitochondrial mass, oxygen consumption rates and cellular respiration, which is consistent with enhanced mitochondrial respiratory function, in GRK2 overexpressing skeletal muscle cells. Increased oxygen consumption was also associated with reduced ECAR in GRK2 overexpressing myoblasts. Similar results have been observed previously in myoblast cultures (10) and suggests that these cells rely on oxidative phosphorylation, as opposed to glycolysis, to meet cellular energy demands. In contrast, upon Mstn addition to control cells, we observed significantly decreased oxygen consumption in muscle cells (Fig. 3F). In addition to reduced basal mitochondrial respiration, Mstn treatment led to significantly reduced maximal mitochondrial respiration when compared to controls. This could indicate diminished availability of substrate (although comparable medium constituents are maintained across all cell cultures), disruption of the electron transport chain or reduced mitochondrial mass (22). In agreement with this, reduced mitochondrial mass was seen in response to Mstn treatment of C2C12 cells (Fig. 2C). Together with reduced maximal respiration we also noted reduced spare respiratory capacity upon Mstn treatment, which suggests that Mstn treated cells may have reduced ability to respond to increased energy demand, when compared to control cells. We further observed reduced ATP-linked respiration upon Mstn treatment, which could indicate a reduced requirement for ATP, reduced availability of substrate or importantly, impaired function of the electron transport chain and subsequent oxidative phosphorylation (22). Moreover, reduced OCR and a concomitant increase in ECAR was noted in Mstn treated cells, consistent with a switch from predominantly aerobic respiration to glycolysis in these cells. Taken together, these observations are consistent with previously published work, revealing

529 that excess Mstn leads to mitochondrial dysfunction and reduced oxygen consumption
530 (39). Unexpectedly, despite increased mitochondrial mass we did not find a rescue of
531 Mstn-mediated impairment of oxygen consumption and cellular respiration upon
532 overexpression of GRK2, although a very minor rescue of maximal respiration and
533 related spare respiratory capacity was noted. Taken together, these data suggest that
534 overexpression of GRK2 is not able to compensate for the deleterious effect of Mstn on
535 mitochondrial respiration, and due to the increased mitochondrial mass noted,
536 conceivably leads to an accumulation of dysfunctional mitochondrial in these cells.
537 Increased expression of OXPHOS genes (Subunits of Complex I and IV) was
538 noted in both Mstn treated control cells (albeit not statistically significant) and Mstn
539 treated GRK2 overexpressing cells. A similar increase in complex IV OXPHOS gene
540 expression has been observed in fibroblasts derived from patients with ATP synthase
541 deficiency, independently of changes in mtDNA (21). Moreover, increased mRNA
542 expression of OXPHOS genes has been noted in diseases associated with additional
543 mitochondrial complex deficiencies (57). Therefore, we speculate that the increased
544 mRNA expression of OXPHOS genes observed in Mstn treated cells may act to
545 compensate for the reduced oxygen consumption/mitochondrial respiration noted in
546 response to Mstn treatment.
547 It is noteworthy to mention that a more pronounced increase in OXPHOS gene
548 expression was observed in GRK2-overexpressing cells following Mstn treatment.
549 Previous work by Sorriento *et al.* (2013) have revealed that macrophages treated with
550 LPS exhibit enhanced translocation and accumulation of GRK2 in mitochondria, which
551 in turn was associated with elevated expression of cytochrome b and NADHd (complex
552 III and I, respectively) (65). This may help to explain the OXPHOS gene expression
553 pattern noted in Mstn treated GRK2 overexpressing myoblasts. However, further
554 studies will need to be undertaken to confirm this hypothesis.
555 In eukaryotic cells, mitochondrial content is tightly controlled through pathways
556 that modulate mitochondrial biogenesis and mitochondrial clearance
557 (autophagy/mitophagy) (8). Mstn robustly increases autophagic flux in myoblasts (Fig.
558 3E). Moreover, we further find that Mstn treatment leads to mitochondrial
559 fragmentation (Fig. 3D), impaired mitochondrial respiration (Fig. 3F & 3G) and a
560 reduction in mitochondrial mass (Fig. 2C). Taken together these data suggest that Mstn
561 treatment disrupts mitochondrial respiration and leads to decreased mitochondrial mass
562 in muscle cells. It is important to mention that while the increased autophagic flux and

563 decreased mitochondrial mass is consistent with enhanced autophagy-mediated
564 mitochondria clearance or mitophagy, a more direct measure of mitophagy would need
565 to be performed to confirm this. Interestingly, GRK2-overexpressing cells, when
566 treated with Mstn, exhibited decreased autophagic flux, which was supported by
567 reduced chloroquine-mediated accumulation of LC3-II and p62 in response to Mstn
568 treatment, when compared to controls. These data suggest that overexpression of
569 GRK2 blocks the overt-autophagic flux induced by Mstn treatment, which would most
570 certainly account for the increased mitochondrial content observed in Mstn treated
571 GRK2 overexpressing myoblasts (Fig. 2C). Furthermore, given that GRK2 reduces
572 autophagic flux in myoblasts and that Mstn treatment leads to a reduction in GRK2
573 protein levels in muscle cells, it is interesting to surmise that Mstn may repress GRK2
574 protein to facilitate autophagy-mediated clearance of mitochondria. However, further
575 work will need to be undertaken to validate this mechanism in muscle cells.
576 The processes of mitochondrial fusion and fission are tightly regulated and are
577 critically involved in governing mitochondria turnover, as evidenced by previous work
578 (71). Here, we show that GRK2-overexpressing cells exhibited increased levels of both
579 mitochondrial fusion (Mfn1/2) and fission (Fis1) proteins, suggesting that
580 overexpression of GRK2 promotes increased mitochondrial fission/fusion, which is
581 consistent with recent work assessing GRK2 function during ionizing radiation-induced
582 mitochondrial damage (16). In contrast to this, Mstn treatment tended to decrease the
583 levels of both Mfn1 and Mfn2 in both control and GRK2 overexpressing myoblasts,
584 suggesting that Mstn treatment may impair mitochondrial fusion. In addition, Mstn
585 treatment led to elevated levels of the mitochondrial fission markers Drp1 and Fis1.
586 However, it is interesting to note that while elevated Fis1 levels were maintained in
587 Mstn treated GRK2 overexpressing myoblasts the Mstn-mediated increase in Drp1 was
588 ablated in GRK2-overexpressing cells, revealing that GRK2 may have an inhibitory role
589 in controlling Drp1 levels. Furthermore, given that Mstn treatment leads to elevated
590 Drp1 and Fis1 (Fig. 3A & 3B) and that overexpression of GRK2 increases the
591 expression of Fis1, but not Drp1 (Fig. 3A & 3B), we propose that the changes in
592 mitochondrial dynamics observed in response to either Mstn treatment or GRK2
593 overexpression may occur through distinct mechanisms. Consistent with this, recent
594 studies have revealed that Fis1 can regulate mitochondrial morphology independently of
595 Drp1 (50).

596 It is important to mention that despite differential regulation of fusion and fission
597 proteins by Mstn and GRK2, a similar reduction in mitochondrial interconnectivity,
598 consistent with increased mitochondrial fragmentation, was noted between GRK2
599 overexpressing myoblasts and Mstn treated control and GRK2 overexpressing cells,
600 when compared to untreated controls (Fig. 3D). Importantly, despite a similar level of
601 mitochondrial fragmentation, overexpression of GRK2 alone led to increased
602 mitochondrial respiration. We propose that the differences in mitochondrial respiration
603 observed may be linked to maintenance of mitochondrial membrane potential in GRK2
604 overexpressing cells. Most certainly, previous work has revealed that fragmentation of
605 mitochondria does not necessarily lead to reduced membrane potential (47) and more
606 importantly, overexpression of GRK2 has been linked with maintenance of
607 mitochondrial membrane potential in HEK293 cells in response to ionizing radiation-
608 induced damage (16). Moreover, we find that the levels of the E3 ligase Parkin, which
609 is recruited to damaged/defective mitochondria with low membrane potential to mediate
610 their removal by autophagosomes (48), remained unchanged in control GRK2
611 overexpressing cells.
612 In conclusion, here we have described a beneficial role for GRK2 in regulating
613 mitochondrial respiratory function and further reveal that excess GRK2 is able to
614 influence autophagic flux in skeletal muscle cells (Fig. 4). Although GRK2 has
615 previously been shown to have a protective role in response to acute mitochondrial
616 damage (16), we find that GRK2 is unable to prevent the significant deleterious effects
617 of Mstn treatment on mitochondrial respiration in muscle cells (Fig. 4).

List of abbreviations used

adenosine triphosphate (ATP)
carbonyl cyanide-p-trifluoromethoxyphenylhydrazone (FCCP)
delta delta cycle threshold (ΔΔCT)
deoxyribonucleic acid (DNA)
dulbecco's modified Eagle's medium (DMEM)
dynamin related protein 1 (Drp1)
electron transport chain (ETC)
epoxomicin (Epox)
extracellular acidification rate (ECAR)
fetal bovine serum (FBS)
forkhead box O (FoxO)
g protein-coupled receptor kinases (GRKs)
glyceraldehyde 3-phosphate dehydrogenase (GAPDH)
growth differentiation factor (GDF)
Henrietta Lacks (HeLa)
horse serum (HS)
horseradish Peroxidase (HRP)
human embryonic kidney 293 (HEK)
insulin-like growth factor (IGF)
interferon gamma (IFN-γ)
interleukin 1β (IL-1β)
lipopolysaccharide (LPS)
microtubule-associated protein-light chain 3 (LC3)
mitochondrial DNA (mtDNA)
mitofusin 1 (Mfn1)
mitofusin 2 (Mfn2)
muscle atrophy f-box (MAFbx)
muscle ringer finger 1 (MuRF1)
myostatin (Mstn)
nicotinamide adenine dinucleotide dehydrogenase (NADHd)
oxidative phosphorylation (OXPHOS)
oxygen consumption rate (OCR)
penicillin/streptomycin (P/S)
phenylmethylsulfoxide (PMSF)
phosphatidyinositol 3 phosphate kinase (PI3K)
polymerase chain reaction (PCR)
quantitative real-time PCR (qPCR)
reactive oxygen species (ROS)
ribonucleic acid (RNA)
small mother against decapentaplegic homolog (SMAD)
standard error of mean (SEM)
transforming growth factor-β (TGF-β)
tris-buffered saline-Tween 20 (TBST)
tumor necrosis alpha (TNF-α)
ubiquitin proteasome pathway (UPP)
uncoupling protein (UCP)
β-adrenergic receptor (β-AR)

Competing Interests

The author(s) declare that they have no competing interests

Authors' contributions

LHM undertook molecular and cell biological studies, participated in design of the study, analyzed and interpreted data and drafted the manuscript. JAYL planned experiments, carried out Western Blot analysis and analyzed and interpreted data. NP planned experiments, carried out mitotracker green staining and seahorse OCR analysis and analyzed and interpreted the data. RKD performed analyses of mitochondrial morphology, interpreted the data and edited the manuscript. CM participated in designing and coordinating the study, analyzed and interpreted all data and drafted the manuscript. All authors read and approved the final manuscript.

Acknowledgements

Thanks to Dr Ravi Kambadur and Dr Mridula Sharma for helpful discussions. Further thanks to Dr. Piyush Khandelia and Dr. Eugene Makeyev for providing the PEM777 vector used in the current study. This study was funded by the Agency for Science, Technology and Research (A*STAR), Singapore and partially funded by NIH grants GM103554 and NS105783-01 (to RKD). We are also indebted to Coordenação de Aperfeiçoamento de Pessoal de Nível Superior (5662-13-3), Conselho Nacional de Desenvolvimento Científico e Tecnológico and Fundação de Amparo à Pesquisa do Estado de São Paulo, Brazil for financial support.

692 # References

693

694 1. **Allen DL, Cleary AS, Lindsay SF, Loh AS, and Reed JM**. Myostatin expression is increased
695 by food deprivation in a muscle-specific manner and contributes to muscle atrophy during
696 prolonged food deprivation in mice. *J Appl Physiol (1985)* 109: 692-701, 2010.
697 2. **Bodine SC, Latres E, Baumhueter S, Lai VK, Nunez L, Clarke BA, Poueymirou WT, Panaro**
698 **FJ, Na E, Dharmarajan K, Pan ZQ, Valenzuela DM, DeChiara TM, Stitt TN, Yancopoulos**
699 **GD, and Glass DJ**. Identification of ubiquitin ligases required for skeletal muscle atrophy.
700 *Science (New York, NY)* 294: 1704-1708, 2001.
701 3. **Boveris A, Oshino N, and Chance B**. The cellular production of hydrogen peroxide.
702 *Biochem J* 128: 617-630, 1972.
703 4. **Chacko BK, Kramer PA, Ravi S, Benavides GA, Mitchell T, Dranka BP, Ferrick D, Singal AK,**
704 **Ballinger SW, Bailey SM, Hardy RW, Zhang J, Zhi D, and Darley-Usmar VM**. The
705 Bioenergetic Health Index: a new concept in mitochondrial translational research. *Clin Sci*
706 *(Lond)* 127: 367-373, 2014.
707 5. **Chuang Y-C, Liou C-W, Chen S-D, Wang P-W, Chuang J-H, Tiao M-M, Hsu T-Y, Lin H-Y, and**
708 **Lin T-K**. Mitochondrial Transfer from Wharton's Jelly Mesenchymal Stem Cell to MERRF
709 Cybrid Reduces Oxidative Stress and Improves Mitochondrial Bioenergetics. *Oxid Med Cell*
710 *Longev* 2017: 5691215-5691215, 2017.
711 6. **Dagda RK, Cherra SJ, 3rd, Kulich SM, Tandon A, Park D, and Chu CT**. Loss of PINK1
712 function promotes mitophagy through effects on oxidative stress and mitochondrial
713 fission. *The Journal of biological chemistry* 284: 13843-13855, 2009.
714 7. **Desler C, Hansen TL, Frederiksen JB, Marcker ML, Singh KK, and Juel Rasmussen L**. Is
715 There a Link between Mitochondrial Reserve Respiratory Capacity and Aging? *Journal of*
716 *Aging Research* 2012: 9, 2012.
717 8. **Diaz F, and Moraes CT**. Mitochondrial biogenesis and turnover. *Cell Calcium* 44: 24-35,
718 2008.
719 9. **Dionyssiou MG, Salma J, Bevzyuk M, Wales S, Zakharyan L, and McDermott JC**. Krüppel-
720 like factor 6 (KLF6) promotes cell proliferation in skeletal myoblasts in response to
721 TGFβ/Smad3 signaling. *Skeletal Muscle* 3: 7, 2013.
722 10. **Dott W, Mistry P, Wright J, Cain K, and Herbert KE**. Modulation of mitochondrial
723 bioenergetics in a skeletal muscle cell line model of mitochondrial toxicity. *Redox Biol* 2:
724 224-233, 2014.
725 11. **Egerman MA, Cadena SM, Gilbert JA, Meyer A, Nelson HN, Swalley SE, Mallozzi C, Jacobi**
726 **C, Jennings LL, Clay I, Laurent G, Ma S, Brachat S, Lach-Trifilieff E, Shavlakadze T,**
727 **Trendelenburg AU, Brack AS, and Glass DJ**. GDF11 Increases with Age and Inhibits
728 Skeletal Muscle Regeneration. *Cell metabolism* 2015.
729 12. **Egerman MA, and Glass DJ**. Signaling pathways controlling skeletal muscle mass. *Critical*
730 *reviews in biochemistry and molecular biology* 49: 59-68, 2014.
731 13. **Eijkelkamp N, Heijnen CJ, Willemen HL, Deumens R, Joosten EA, Kleibeuker W, den**
732 **Hartog IJ, van Velthoven CT, Nijboer C, Nassar MA, Dorn GW, 2nd, Wood JN, and**
733 **Kavelaars A**. GRK2: a novel cell-specific regulator of severity and duration of inflammatory
734 pain. *The Journal of neuroscience : the official journal of the Society for Neuroscience* 30:
735 2138-2149, 2010.
736 14. **Ferrick DA, Neilson A, and Beeson C**. Advances in measuring cellular bioenergetics using
737 extracellular flux. *Drug discovery today* 13: 268-274, 2008.
738 15. **Ferrick DA, Neilson A, and Beeson C**. Advances in measuring cellular bioenergetics using
739 extracellular flux. *Drug discovery today* 13: 268-274, 2008.
740 16. **Franco A, Sorriento D, Gambardella J, Pacelli R, Prevete N, Procaccini C, Matarese G,**
741 **Trimarco B, Iaccarino G, and Ciccarelli M**. GRK2 moderates the acute mitochondrial

damage to ionizing radiation exposure by promoting mitochondrial fission/fusion. *Cell Death Discov* 4: 25, 2018.

17. **Fu D, Lala-Tabbert N, Lee H, and Wiper-Bergeron N**. Mdm2 promotes myogenesis through the ubiquitination and degradation of CCAAT/enhancer-binding protein β. *The Journal of biological chemistry* 290: 10200-10207, 2015.
18. **Fusco A, Santulli G, Sorriento D, Cipolletta E, Garbi C, Dorn GW, 2nd, Trimarco B, Feliciello A, and Iaccarino G**. Mitochondrial localization unveils a novel role for GRK2 in organelle biogenesis. *Cellular signalling* 24: 468-475, 2012.
19. **Garcia I, Innis-Whitehouse W, Lopez A, Keniry M, and Gilkerson R**. Oxidative insults disrupt OPA1-mediated mitochondrial dynamics in cultured mammalian cells. *Redox Report* 23: 160-167, 2018.
20. **Ge X, Sathiakumar D, Lua BJG, Kukreti H, Lee M, and McFarlane C**. Myostatin signals through miR-34a to regulate Fndc5 expression and browning of white adipocytes. *International Journal Of Obesity* 41: 137, 2016.
21. **Havlickova Karbanova V, Cizkova Vrbacka A, Hejzlarova K, Nuskova H, Stranecky V, Potocka A, Kmoch S, and Houstek J**. Compensatory upregulation of respiratory chain complexes III and IV in isolated deficiency of ATP synthase due to TMEM70 mutation. *Biochimica et biophysica acta* 1817: 1037-1043, 2012.
22. **Hill BG, Benavides GA, Lancaster JR, Jr., Ballinger S, Dell'Italia L, Jianhua Z, and Darley-Usmar VM**. Integration of cellular bioenergetics with mitochondrial quality control and autophagy. *Biol Chem* 393: 1485-1512, 2012.
23. **Ho J, Cocolakis E, Dumas VM, Posner BI, Laporte SA, and Lebrun JJ**. The G protein-coupled receptor kinase-2 is a TGFbeta-inducible antagonist of TGFbeta signal transduction. *The EMBO journal* 24: 3247-3258, 2005.
24. **Huang Z, Chen X, and Chen D**. Myostatin: A novel insight into its role in metabolism, signal pathways, and expression regulation. *Cellular signalling* 23: 1441-1446, 2011.
25. **Jacobi D, Liu S, Burkewitz K, Kory N, Knudsen NH, Alexander RK, Unluturk U, Li X, Kong X, Hyde AL, Gangl MR, Mair WB, and Lee CH**. Hepatic Bmal1 Regulates Rhythmic Mitochondrial Dynamics and Promotes Metabolic Fitness. *Cell metabolism* 22: 709-720, 2015.
26. **Jimenez-Sainz MC, Murga C, Kavelaars A, Jurado-Pueyo M, Krakstad BF, Heijnen CJ, Mayor F, Jr., and Aragay AM**. G protein-coupled receptor kinase 2 negatively regulates chemokine signaling at a level downstream from G protein subunits. *Molecular biology of the cell* 17: 25-31, 2006.
27. **Joulia D, Bernardi H, Garandel V, Rabenoelina F, Vernus B, and Cabello G**. Mechanisms involved in the inhibition of myoblast proliferation and differentiation by myostatin. *Experimental cell research* 286: 263-275, 2003.
28. **Khandelia P, Yap K, and Makeyev EV**. Streamlined platform for short hairpin RNA interference and transgenesis in cultured mammalian cells. *Proceedings of the National Academy of Sciences of the United States of America* 108: 12799-12804, 2011.
29. **Kisselev AF, and Goldberg AL**. Proteasome inhibitors: from research tools to drug candidates. *Chem Biol* 8: 739-758, 2001.
30. **Klionsky DJ, Abdelmohsen K, Abe A, Abedin MJ, Abeliovich H, Acevedo Arozena A, Adachi H, Adams CM, Adams PD, Adeli K, Adhihetty PJ, Adler SG, Agam G, Agarwal R, Aghi MK, Agnello M, Agostinis P, Aguilar PV, et al.** Guidelines for the use and interpretation of assays for monitoring autophagy (3rd edition). *Autophagy* 12: 1-222, 2016.
31. **Koukourakis MI, Kalamida D, Giatromanolaki A, Zois CE, Sivridis E, Pouliliou S, Mitrakas A, Gatter KC, and Harris AL**. Autophagosome Proteins LC3A, LC3B and LC3C Have Distinct Subcellular Distribution Kinetics and Expression in Cancer Cell Lines. *PLoS One* 10: e0137675, 2015.

32. **Lach-Trifilieff E, Minetti GC, Sheppard K, Ibebunjo C, Feige JN, Hartmann S, Brachat S, Rivet H, Koelbing C, Morvan F, Hatakeyama S, and Glass DJ**. An antibody blocking activin type II receptors induces strong skeletal muscle hypertrophy and protects from atrophy. *Molecular and cellular biology* 34: 606-618, 2014.
33. **Langley B, Thomas M, Bishop A, Sharma M, Gilmour S, and Kambadur R**. Myostatin inhibits myoblast differentiation by down-regulating MyoD expression. *The Journal of biological chemistry* 277: 49831-49840, 2002.
34. **Lecker SH, Goldberg AL, and Mitch WE**. Protein degradation by the ubiquitin-proteasome pathway in normal and disease states. *J Am Soc Nephrol* 17: 1807-1819, 2006.
35. **Lee JY, Hopkinson NS, and Kemp PR**. Myostatin induces autophagy in skeletal muscle in vitro. *Biochemical and biophysical research communications* 415: 632-636, 2011.
36. **Li S, Wang J, Zhou A, Khan FA, Hu L, and Zhang S**. Porcine reproductive and respiratory syndrome virus triggers mitochondrial fission and mitophagy to attenuate apoptosis. *Oncotarget* 7: 56002-56012, 2016.
37. **Lin JR, Shen WL, Yan C, and Gao PJ**. Downregulation of dynamin-related protein 1 contributes to impaired autophagic flux and angiogenic function in senescent endothelial cells. *Arterioscler Thromb Vasc Biol* 35: 1413-1422, 2015.
38. **Liu P, Osawa S, and Weiss ER**. M opsin phosphorylation in intact mammalian retinas. *Journal of Neurochemistry* 93: 135-144, 2005.
39. **Liu Y, Cheng H, Zhou Y, Zhu Y, Bian R, Chen Y, Li C, Ma Q, Zheng Q, Zhang Y, Jin H, Wang X, Chen Q, and Zhu D**. Myostatin induces mitochondrial metabolic alteration and typical apoptosis in cancer cells. *Cell Death Dis* 4: e494, 2013.
40. **Lokireddy S, Mouly V, Butler-Browne G, Gluckman PD, Sharma M, Kambadur R, and McFarlane C**. Myostatin promotes the wasting of human myoblast cultures through promoting ubiquitin-proteasome pathway-mediated loss of sarcomeric proteins. *American journal of physiology Cell physiology* 301: C1316-1324, 2011.
41. **Lorenz K, Stathopoulou K, Schmid E, Eder P, and Cuello F**. Heart failure-specific changes in protein kinase signalling. *Pflugers Archiv : European journal of physiology* 466: 1151-1162, 2014.
42. **Ma K, Mallidis C, Bhasin S, Mahabadi V, Artaza J, Gonzalez-Cadavid N, Arias J, and Salehian B**. Glucocorticoid-induced skeletal muscle atrophy is associated with upregulation of myostatin gene expression. *American journal of physiology Endocrinology and metabolism* 285: E363-371, 2003.
43. **McFarlane C, Hennebry A, Thomas M, Plummer E, Ling N, Sharma M, and Kambadur R**. Myostatin signals through Pax7 to regulate satellite cell self-renewal. *Experimental cell research* 314: 317-329, 2008.
44. **McFarlane C, Plummer E, Thomas M, Hennebry A, Ashby M, Ling N, Smith H, Sharma M, and Kambadur R**. Myostatin induces cachexia by activating the ubiquitin proteolytic system through an NF-kappaB-independent, FoxO1-dependent mechanism. *Journal of cellular physiology* 209: 501-514, 2006.
45. **McPherron AC, Lawler AM, and Lee SJ**. Regulation of skeletal muscle mass in mice by a new TGF-beta superfamily member. *Nature* 387: 83-90, 1997.
46. **Mukherjee A, Patra U, Bhowmick R, and Chawla-Sarkar M**. Rotaviral nonstructural protein 4 triggers dynamin-related protein 1-dependent mitochondrial fragmentation during infection. *Cell Microbiol* 20: e12831, 2018.
47. **Nakamura K, Nemani VM, Azarbal F, Skibinski G, Levy JM, Egami K, Munishkina L, Zhang J, Gardner B, Wakabayashi J, Sesaki H, Cheng Y, Finkbeiner S, Nussbaum RL, Masliah E, and Edwards RH**. Direct membrane association drives mitochondrial fission by the Parkinson disease-associated protein alpha-synuclein. *The Journal of biological chemistry* 286: 20710-20726, 2011.
48. **Narendra D, Tanaka A, Suen D-F, and Youle RJ**. Parkin is recruited selectively to impaired mitochondria and promotes their autophagy. *J Cell Biol* 183: 795-803, 2008.

49. **Oliver E, Flacco N, Arce C, Ivorra MD, D'Ocon MP, and Noguera MA**. Changes in adrenoceptors and G-protein-coupled receptor kinase 2 in L-NAME-induced hypertension compared to spontaneous hypertension in rats. *Journal of vascular research* 51: 209-220, 2014.
50. **Onoue K, Jofuku A, Ban-Ishihara R, Ishihara T, Maeda M, Koshiba T, Itoh T, Fukuda M, Otera H, Oka T, Takano H, Mizushima N, Mihara K, and Ishihara N**. Fis1 acts as a mitochondrial recruitment factor for TBC1D15 that is involved in regulation of mitochondrial morphology. *J Cell Sci* 126: 176-185, 2013.
51. **Pankiv S, Clausen TH, Lamark T, Brech A, Bruun JA, Outzen H, Overvatn A, Bjorkoy G, and Johansen T**. p62/SQSTM1 binds directly to Atg8/LC3 to facilitate degradation of ubiquitinated protein aggregates by autophagy. *The Journal of biological chemistry* 282: 24131-24145, 2007.
52. **Peker N, Donipadi V, Sharma M, McFarlane C, and Kambadur R**. Loss of Parkin impairs mitochondrial function and leads to muscle atrophy. *American journal of physiology Cell physiology* 315: C164-C185, 2018.
53. **Penela P, Murga C, Ribas C, Lafarga V, and Mayor F, Jr.** The complex G protein-coupled receptor kinase 2 (GRK2) interactome unveils new physiopathological targets. *British journal of pharmacology* 160: 821-832, 2010.
54. **Penela P, Ribas C, and Mayor F**. Mechanisms of regulation of the expression and function of G protein-coupled receptor kinases. *Cellular signalling* 15: 973-981, 2003.
55. **Premont RT, and Gainetdinov RR**. Physiological Roles of G Protein–Coupled Receptor Kinases and Arrestins. *Annual Review of Physiology* 69: 511-534, 2007.
56. **Reardon KA, Davis J, Kapsa RM, Choong P, and Byrne E**. Myostatin, insulin-like growth factor-1, and leukemia inhibitory factor mRNAs are upregulated in chronic human disuse muscle atrophy. *Muscle Nerve* 24: 893-899, 2001.
57. **Reinecke F, Smeitink JAM, and van der Westhuizen FH**. OXPHOS gene expression and control in mitochondrial disorders. *Biochimica et Biophysica Acta (BBA) - Molecular Basis of Disease* 1792: 1113-1121, 2009.
58. **Rios R, Carneiro I, Arce VM, and Devesa J**. Myostatin regulates cell survival during C2C12 myogenesis. *Biochemical and biophysical research communications* 280: 561-566, 2001.
59. **Sacoman JL, Dagda RY, Burnham-Marusich AR, Dagda RK, and Berninsone PM**. Mitochondrial O-GlcNAc Transferase (mOGT) Regulates Mitochondrial Structure, Function, and Survival in HeLa Cells. *The Journal of biological chemistry* 292: 4499-4518, 2017.
60. **Salcedo A, Mayor F, Jr., and Penela P**. Mdm2 is involved in the ubiquitination and degradation of G-protein-coupled receptor kinase 2. *The EMBO journal* 25: 4752-4762, 2006.
61. **Schlegel P, Reinkober J, Meinhardt E, Tscheschner H, Gao E, Schumacher SM, Yuan A, Backs J, Most P, Wieland T, Koch WJ, Katus HA, and Raake PW**. G protein-coupled receptor kinase 2 promotes cardiac hypertrophy. *PLoS One* 12: e0182110, 2017.
62. **Sharma M, Kambadur R, Matthews KG, Somers WG, Devlin GP, Conaglen JV, Fowke PJ, and Bass JJ**. Myostatin, a transforming growth factor-beta superfamily member, is expressed in heart muscle and is upregulated in cardiomyocytes after infarct. *Journal of cellular physiology* 180: 1-9, 1999.
63. **Shenoy SK, and Lefkowitz RJ**. Receptor regulation: beta-arrestin moves up a notch. *Nature cell biology* 7: 1159-1161, 2005.
64. **Shintani T, and Klionsky DJ**. Cargo proteins facilitate the formation of transport vesicles in the cytoplasm to vacuole targeting pathway. *The Journal of biological chemistry* 279: 29889-29894, 2004.
65. **Sorriento D, Fusco A, Ciccarelli M, Rungi A, Anastasio A, Carillo A, Dorn GW, 2nd, Trimarco B, and Iaccarino G**. Mitochondrial G protein coupled receptor kinase 2 regulates proinflammatory responses in macrophages. *FEBS letters* 587: 3487-3494, 2013.

66. **Sripathi SR, He W, Sylvester OD, Neksumi M, Um J-Y, Dluya T, Bernstein PS, and Jahng WJ**. Altered Cytoskeleton as a Mitochondrial Decay Signature in the Retinal Pigment Epithelium. *Protein J* 35: 179-192, 2016.
67. **Tan J, Xie Q, Song S, Miao Y, and Zhang Q**. Albumin Overload and PINK1/Parkin Signaling-Related Mitophagy in Renal Tubular Epithelial Cells. *Med Sci Monit* 24: 1258-1267, 2018.
68. **Tanida I**. Autophagosome formation and molecular mechanism of autophagy. *Antioxidants & redox signaling* 14: 2201-2214, 2011.
69. **Thomas M, Langley B, Berry C, Sharma M, Kirk S, Bass J, and Kambadur R**. Myostatin, a negative regulator of muscle growth, functions by inhibiting myoblast proliferation. *The Journal of biological chemistry* 275: 40235-40243, 2000.
70. **Trendelenburg AU, Meyer A, Rohner D, Boyle J, Hatakeyama S, and Glass DJ**. Myostatin reduces Akt/TORC1/p70S6K signaling, inhibiting myoblast differentiation and myotube size. *American journal of physiology Cell physiology* 296: C1258-1270, 2009.
71. **Twig G, Elorza A, Molina AJ, Mohamed H, Wikstrom JD, Walzer G, Stiles L, Haigh SE, Katz S, Las G, Alroy J, Wu M, Py BF, Yuan J, Deeney JT, Corkey BE, and Shirihai OS**. Fission and selective fusion govern mitochondrial segregation and elimination by autophagy. *The EMBO journal* 27: 433-446, 2008.
72. **Usui I, Imamura T, Satoh H, Huang J, Babendure JL, Hupfeld CJ, and Olefsky JM**. GRK2 is an endogenous protein inhibitor of the insulin signaling pathway for glucose transport stimulation. *The EMBO journal* 23: 2821-2829, 2004.
73. **Wang DT, Yang YJ, Huang RH, Zhang ZH, and Lin X**. Myostatin Activates the Ubiquitin-Proteasome and Autophagy-Lysosome Systems Contributing to Muscle Wasting in Chronic Kidney Disease. *Oxid Med Cell Longev* 2015: 684965, 2015.
74. **Wiemerslage L, and Lee D**. Quantification of mitochondrial morphology in neurites of dopaminergic neurons using multiple parameters. *J Neurosci Methods* 262: 56-65, 2016.
75. **Willemen HL, Eijkelkamp N, Garza Carbajal A, Wang H, Mack M, Zijlstra J, Heijnen CJ, and Kavelaars A**. Monocytes/Macrophages control resolution of transient inflammatory pain. *The journal of pain : official journal of the American Pain Society* 15: 496-506, 2014.
76. **Wu CL, Chen CH, Hwang CS, Chen SD, Hwang WC, and Yang DI**. Roles of p62 in BDNF-dependent autophagy suppression and neuroprotection against mitochondrial dysfunction in rat cortical neurons. *J Neurochem* 140: 845-861, 2017.
77. **Yoshii SR, and Mizushima N**. Monitoring and Measuring Autophagy. *Int J Mol Sci* 18: 2017.
78. **Zhang L, Ning Y, Li P, and Zan L**. Smad3 influences Smad2 expression via transcription factor C/EBPalpha and C/EBPbeta during bovine myoblasts differentiation. *Arch Biochem Biophys* 2019.
79. **Zhang W, Shu C, Li Q, Li M, and Li X**. Adiponectin affects vascular smooth muscle cell proliferation and apoptosis through modulation of the mitofusin-2-mediated Ras-Raf-Erk1/2 signaling pathway. *Mol Med Rep* 12: 4703-4707, 2015.

Figure legends

Figure 1: Excess Mstn leads to reduced GRK2 protein levels. (A) *left*: immunoblot (IB) analysis of GRK2 protein expression in C2C12 myotubes after 24h treatment with (+) or without (-) Mstn. Relevant bands from the IB are shown. The levels of GAPDH were assessed as a loading control. *Right:* densitometric analysis of protein levels (GRK2) normalized to GAPDH levels. Values represent mean ± SEM; 5 biological replicates from 3 independent experiments were performed and analyzed; *p<0.05. Student t-test **(B)** IB analysis of GRK2 protein content in both myoblasts (*left*) and myotubes (*right*) treated with (+) or without (-) Mstn over a time course (3, 6, 16, 24 and 48h). The levels of GAPDH were assessed as a loading control. For each myoblast and myotube culture one independent experiment with one biological replicate was performed. **(C)** IB analysis of GRK2 protein levels in the absence (-) or presence (+) of increasing concentrations of Mstn protein (2, 3, 4 and 5µg/ml) in both myoblasts (*left*) and myotubes (*right*). The levels of GAPDH were assessed as a loading control. For each myoblast and myotube culture one independent experiment with one biological replicate was performed. **(D)** IB analysis of GRK2 protein levels in myotubes treated with (+) or without (-) Mstn, in the presence (+) or absence (-) of the proteasome inhibitor MG132 or vehicle control (DMSO). The levels of GAPDH were assessed as a loading control, n=3 biological replicates from one independent experiment. **(E)** IB analysis of GRK2 protein levels in myotubes treated with (+) or without (-) Mstn, in the presence (+) or absence (-) of the proteasome inhibitor Epoxomicin (Epox) or vehicle control (DMSO). The levels of GAPDH were assessed as a loading control. One biological replicate and one independent experiment was performed.

Figure 2: Overexpression of GRK2 leads to increased mitochondrial content in muscle cells. (A) qPCR analysis of *Grk2* expression in stable Control and GRK2 overexpressing C2C12 myotubes (GRK2) treated with (+) or without (-) Mstn for 24h. Gene expression was normalized to the endogenous control, *Gapdh*, using the ΔΔCT method. Values represent mean ± SEM; n=3 biological replicates from one independent experiment; ∗p < 0.05 vs Control - Mstn and #p<0.05 vs. GRK2 - Mstn. One-Way ANOVA with Bonferroni correction was used for multiple comparisons. **(B)** IB analysis of GRK2 protein levels in Control and stable GRK2 overexpressing C2C12 myotubes (GRK2) treated with (+) or without (-) Mstn for 24h. The levels of GAPDH

were assessed as a loading control. Representative of at least 3 independent experiments. **(C)** Graph showing quantitative analysis of mitotracker green staining in Control and stable GRK2 overexpressing myotubes following treatment with (-) or without (-) Mstn. Values represent mean ± SEM (2065± 5 for Control - Mstn, 1863±100 for Control + Mstn, 2491±28 for GRK2 - Mstn and 2949±34 for GRK2 + Mstn); n=3 biological replicates from one independent experiment. ∗p < 0.05 vs. Control - Mstn. #p<0.05 vs. GRK2 - Mstn and &p<0.05 vs. Control + Mstn. One-Way ANOVA with Bonferroni correction was used for multiple comparisons **(D)** qPCR analysis of mitochondrial encoded NADH dehydrogenase 1 (*mt-Nd1*), NADH dehydrogenase 4 (*mt-Nd4*), cytochrome c oxidase I (*mt-Co1),* cytochrome c oxidase II (*mt-Co2*) and cytochrome c oxidase III (*mt-Co3*) expression in Control and stable GRK2 overexpressing C2C12 myotubes (GRK2) treated with (+) or without (-) Mstn for 24h. Gene expression was normalized to the endogenous control, *Gapdh*, using the ΔΔCT method. Values represent mean ± SEM; n = 3 biological replicates from one independent experiment; ∗p < 0.05 vs. Control - Mstn. #p<0.05 vs. GRK2 - Mstn. One-Way ANOVA with Bonferroni correction was used for multiple comparisons

Figure 3: Overexpression of GRK2 in myoblasts enhances mitochondrial respiration and reverses Mstn-induced autophagic flux. **(A)** IB analysis of Mitofusin 1 and 2 (Mfn1/2), Dynamin-related protein 1 (Drp1), mitochondrial fission 1 protein (Fis1) and Parkin protein levels in Control and stable GRK2 overexpressing C2C12 myotubes (GRK2) treated with (+) or without (-) Mstn for 24h. The levels of GAPDH were assessed as a loading control. n=3 biological replicates from one independent experiment. **(B)** Densitometric analysis of IB for Mfn1/2, Drp1, Fis1 and Parkin protein levels, normalized to GAPDH, in Control and stable C2C12 myotubes overexpressing GRK2 (GRK2) treated with (+) or without (-) Mstn for 24h. Values represent mean ± SEM. *p<0.05 vs. Control - Mstn. #p<0.05 vs. GRK2 - Mstn. &p<0.05 vs. Control + Mstn. One-Way ANOVA with Bonferroni correction was used for multiple comparisons **(C)** Representative confocal micrographs of Control and GRK2 overexpressing myoblasts (GRK2) treated with (+) or without (-) Mstn and stained with MitoTracker Red to visualize mitochondria. Nuclei were counterstained with DAPI (Blue). Scale bar represents 40μm. The insert (white box) in the lower left image was zoomed 40% from the original image and the white arrows are pointing to fragmented mitochondria (small and circular). **(D)** Quantitative imaged-based analyses

of mitochondrial interconnectivity ratio [(Area/perimeter)/minor axis] in paraformaldehyde fixed control and GRK2 overexpressing C2C12 cells treated with (+) or without (-) recombinant Mstn protein. The bar graph shows data compiled from a representative experiment (data represents mean values ± SEM, n=20-35 biological replicates per condition from one independent experiment). One-Way ANOVA with Bonferroni correction was used for multiple comparisons. *p< 0.05. **(E)** IB analysis of p62, LC3-I and LC3-II protein levels in control and stable GRK2 overexpressing C2C12 myoblasts (GRK2) co-treated with (+) or without (-) Mstn for 12h in the absence (-) or presence (+) of Chloroquine. The levels of GAPDH were assessed as a loading control. Blots are representative of two independent experiments. **(F)** Graph showing the real-time OCR in Control and stable GRK2 overexpressing C2C12 myotubes (GRK2) treated with (+) or without (-) Mstn, as assessed by the Seahorse XF^e24 extracellular flux analyzer. Time points where Oligomycin (Oligo), FCCP and Antimycin/Rotenone (Ant/Rot) were injected (arrows) and the rate number where each OCR was measured are indicated. Values represent mean ± SEM of three independent measurements from 5 biological replicates. **(G)** Graph showing quantification of basal, maximal, ATP-linked and non-mitochondrial (Non-mito.) respiration, spare respiratory capacity (S.R.C) and respiration due to proton leak in Control and stable GRK2 overexpressing C2C12 myotubes (GRK2) treated with (+) or without (-) Mstn. All OCR values were normalized to total protein. Values represent mean ± SEM of three independent measurements from 5 biological replicates. Two different experiments were performed. *p<0.05 vs. Control - Mstn. #p<0.05 vs. GRK2 - Mstn. &p<0.05 vs. Control + Mstn. One-Way ANOVA with Bonferroni correction was used for multiple comparisons. **(H)** Graph showing OCR vs. ECAR in Control and stable GRK2 overexpressing C2C12 myotubes (GRK2) treated with (+) or without (-) Mstn. Values represent mean ± SEM of three independent measurements from 5 biological replicates. Two different experiments were performed.

Figure 4: GRK2 regulates mitochondrial respiratory function and impairs Mstn-mediated autophagy in muscle cells. Myostatin signaling (red lines and arrows) in muscle cells results in loss of GRK2 protein through a mechanism involving the ubiquitin-proteasome pathway. Furthermore, Mstn treatment leads to increased mitochondrial fragmentation (consistent with mitochondrial fission), impaired mitochondrial respiration and decreased mitochondrial mass, which was associated with

1039 increased autophagic flux in muscle cells. Taken together, we surmise that Mstn may
1040 act to stimulate autophagy-mediated clearance of mitochondria, or mitophagy, in muscle
1041 cells. Overexpression of GRK2 (green lines and arrows), although not able to overcome
1042 Mstn-induced impairment of mitochondrial respiration, blocked the increased
1043 autophagic flux promoted by Mstn. Moreover, elevated GRK2 levels resulted in
1044 mitochondrial fragmentation, which was associated with an increase in both
1045 mitochondrial mass and mitochondrial respiration. Given that overexpression of GRK2
1046 resulted in mitochondrial fragmentation and altered the levels of critical mitochondrial
1047 fusions/fission proteins we speculate a role for GRK2 in regulating the balance between
1048 mitochondria fusion and fission in muscle cells (indicated by the ?). Arrows represent
1049 stimulation and blunt-ended lines represent inhibition.
1050

1051 **Table 1**

1052

Gene Symbol	Forward Primer Sequence	Reverse Primer Sequence
Grk2	AGAGGGACGTCAATCGGAGA	TTGCGGTACAGTTCCTGGTC
mt-Co1	GCACTGGTGGATGCCTTCT	TCTCTCGGGACTCCTTGATGA
mt-Co2	ACGTGCAACACCTGAGCGGT	GAAGGTGTCGGGCAGCAGGG
mt-Co3	CTACCAAGGCCACCACACTC	TCATGCTGCGGCTTCAAATC
mt-Nd1	TCCGAGCATCTTATCCACGC	GTATGGTGGTACTCCCGCTG
mt-Nd4	CCACTGCTAATTGCCCTCAT	CTTCAACATGGGCTTTTGGT
Gapdh	GATGATGACCCGTTTGGCTCC	ACGCTCGTGGAAAGAAAAGA

1053

1054 ***Table 1: Sequences of primers.*** Table displaying gene symbols and forward and reverse

1055 sequences of all primers used in the current study.

Table 2

Antibody	Company	Catalog No.	Dilution	Blocking Solution
anti-GRK2	Santa Cruz	sc-562	1:1000	5% milk
anti-GAPDH	Santa Cruz	sc-32233	1:1000	5% milk
anti-PARKIN	Abcam	ab15954	1:1000	5% milk
anti-MFN1	Abcam	ab126575	1:1000	5% milk
anti-MFN2	Santa Cruz	sc-100560	1:1000	5% milk
anti-FIS1	Santa Cruz	sc-98900	1:500	5% milk
anti-DRP1	Santa Cruz	sc-32898	1:5000	5% milk
anti-P62	Abcam	ab91526	1:5000	5% milk
anti-LC3B	Abcam	NB100-2220	1:500	5% milk
Goat anti-Mouse HRP	Bio-rad	1706516	1:5000	5% milk
Goat anti-Rabbit HRP	Bio-rad	1706515	15000	5% milk

Table 2: Details of antibodies. Table displaying particulars of the antibodies used in the current study. Antibody name, source, catalog number, working dilution and blocking solution are provided.

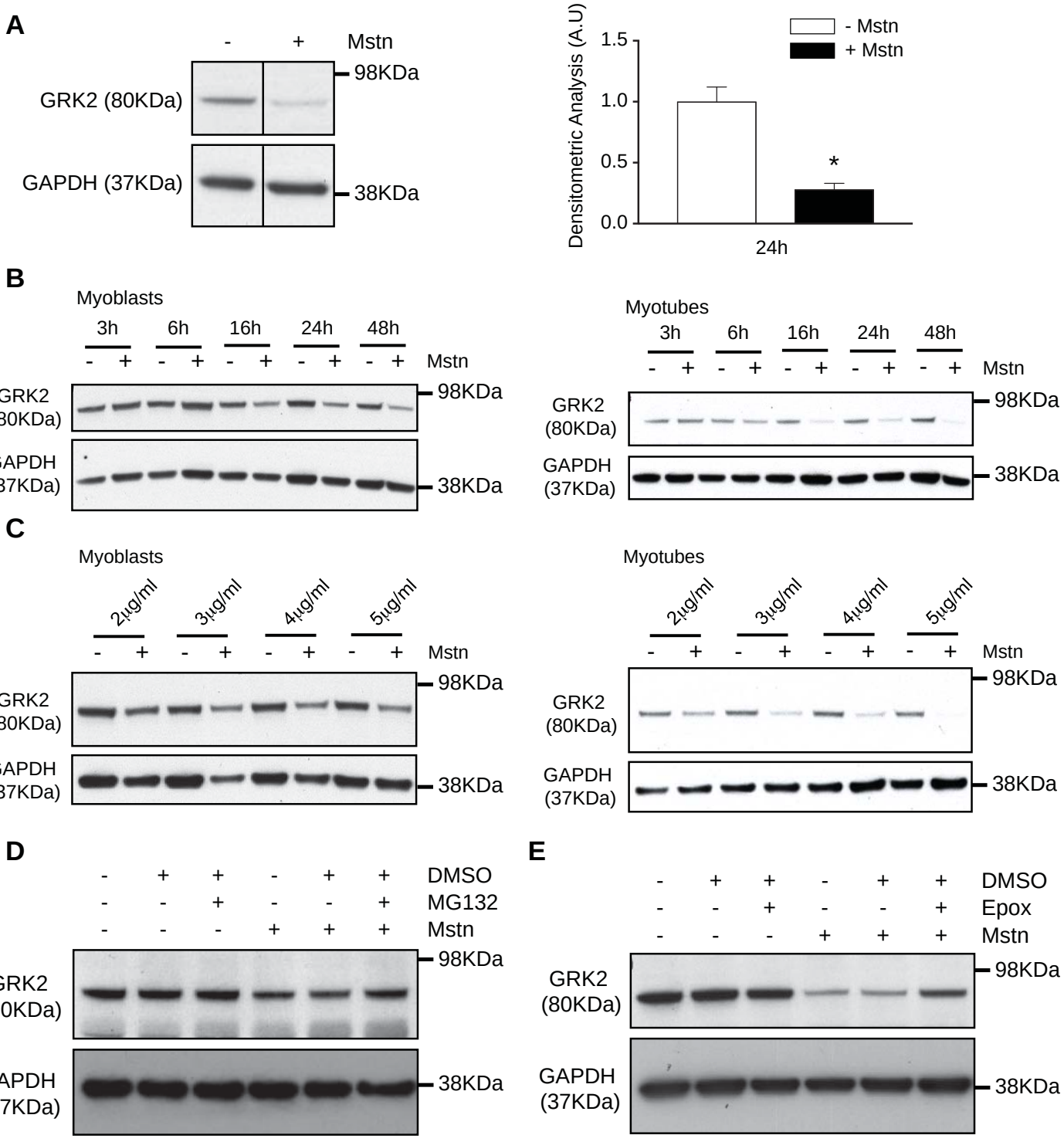

Figure 1

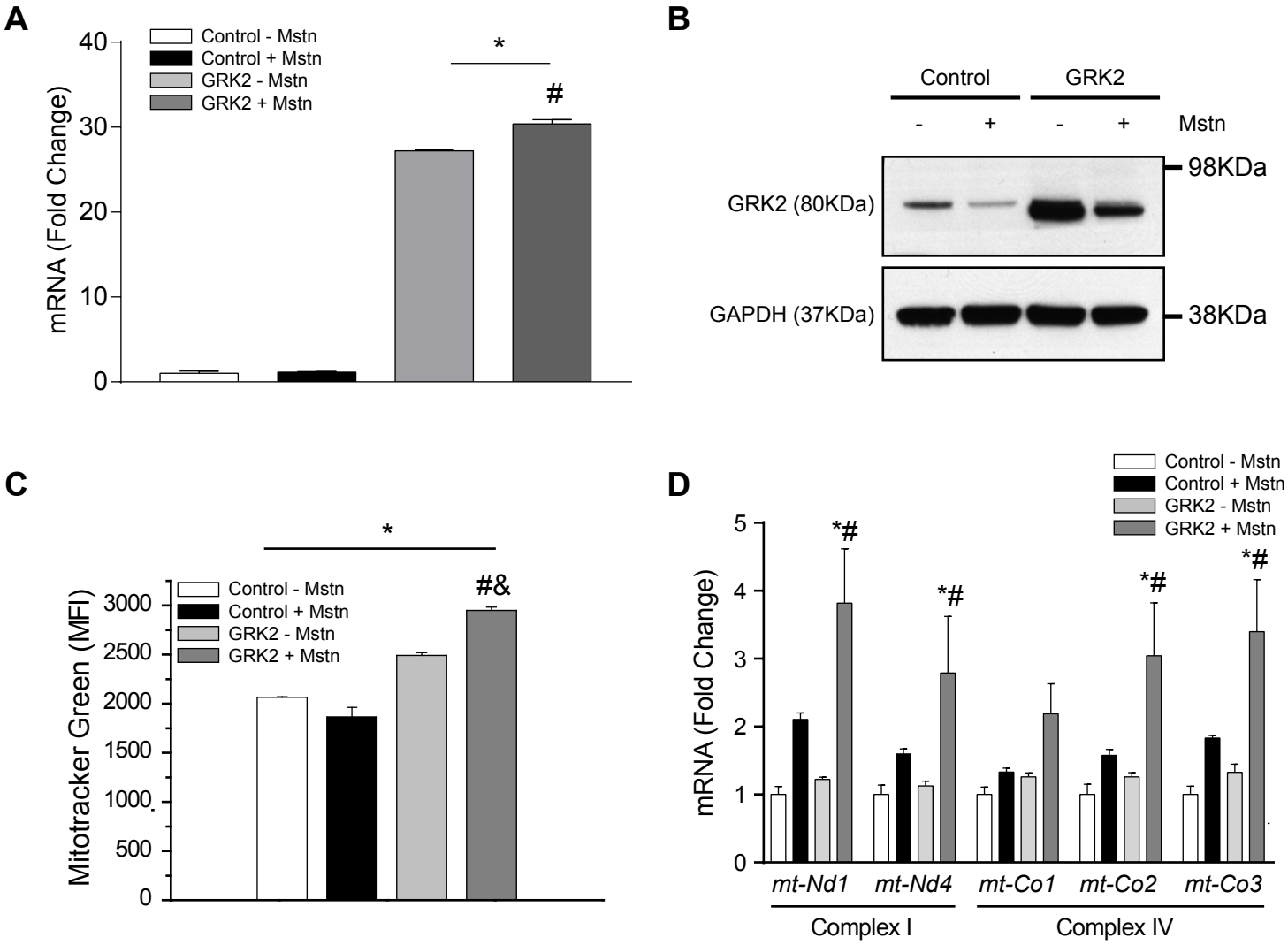

Figure 2

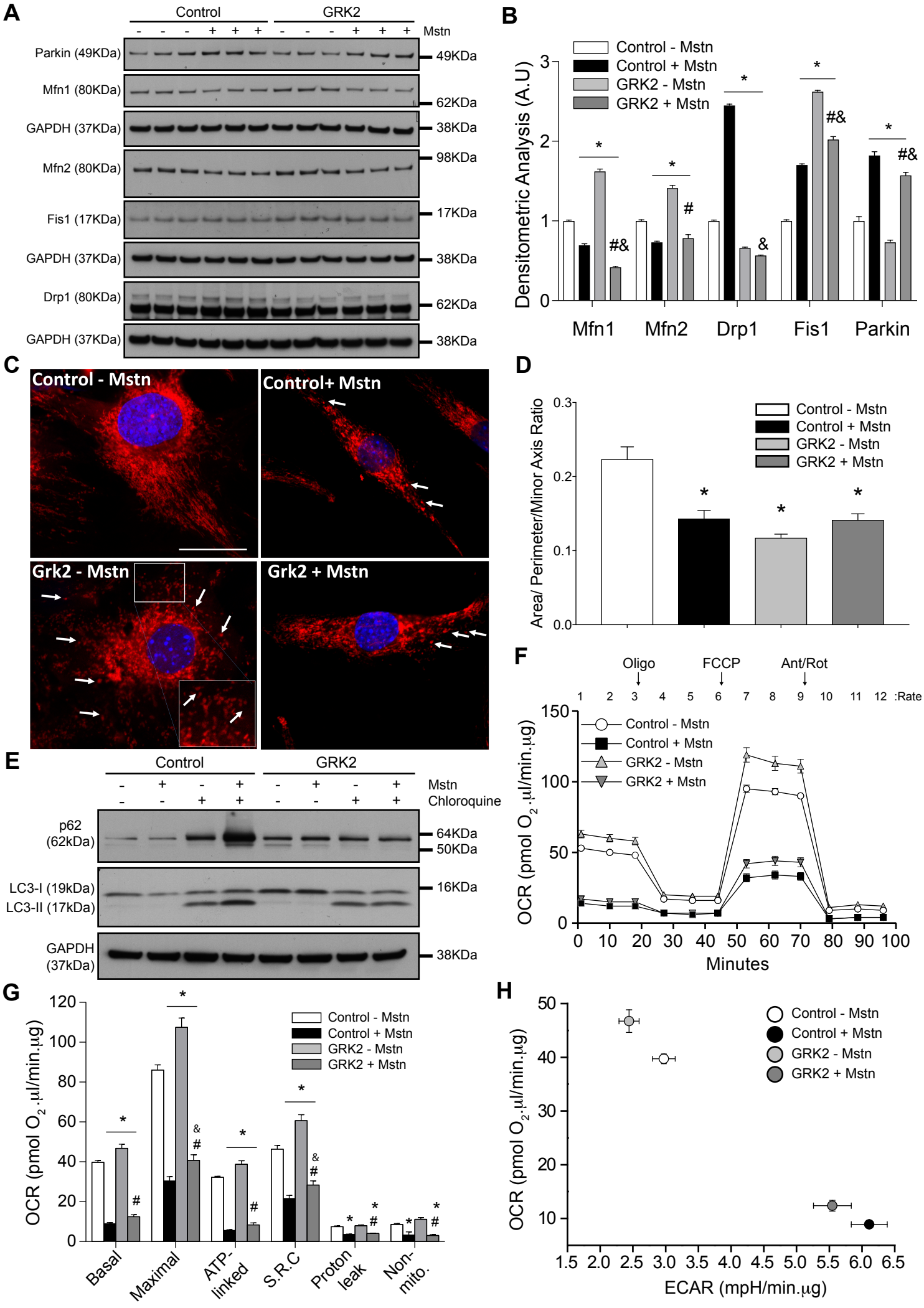

Figure 3

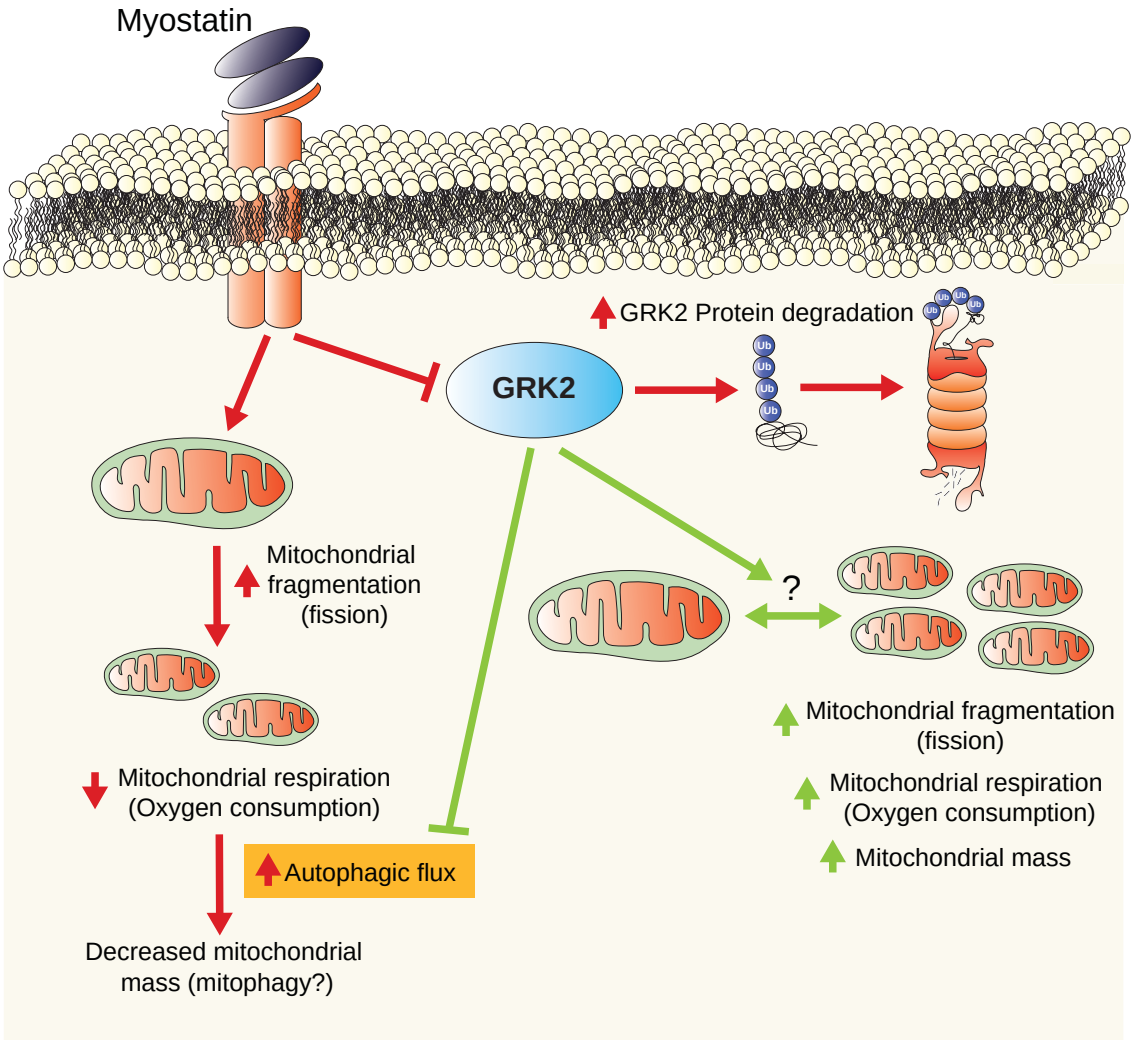

Figure 4